

On Graphene in the Interstellar Medium

DRAFT: 2021.6.1.1022

X.H. Chen^{1,2}, Aigen Li², and Ke Zhang³

ABSTRACT

The possible detection of C₂₄, a planar graphene, recently reported in several planetary nebulae by García-Hernández et al. (2011, 2012) inspires us to explore whether and how much graphene could exist in the interstellar medium (ISM) and how it would reveal its presence through its ultraviolet (UV) extinction and infrared (IR) emission. In principle, interstellar graphene could arise from the photochemical processing of polycyclic aromatic hydrocarbon (PAH) molecules which are abundant in the ISM through a complete loss of their hydrogen atoms, and/or from graphite which is thought to be a major dust species in the ISM through fragmentation caused by grain-grain collisional shattering. Both quantum-chemical computations and laboratory experiments have shown that the exciton-dominated electronic transitions in graphene cause a strong absorption band near 2755 Å. We calculate the UV absorption of graphene and place an upper limit of ~ 5 ppm of C/H (i.e., $\sim 1.9\%$ of the total interstellar C) on the interstellar graphene abundance. We also model the stochastic heating of graphene C₂₄ in the ISM, excited by single starlight photons of the interstellar radiation field and calculate its IR emission spectra. We also derive the abundance of graphene in the ISM to be < 5 ppm of C/H by comparing the model emission spectra with that observed in the ISM.

Subject headings: dust, extinction — ISM: lines and bands — ISM: molecules

¹Department of Physics, Xiangtan University, 411105 Xiangtan, Hunan Province, China

²Department of Physics and Astronomy, University of Missouri, Columbia, MO 65211, USA; lia@missouri.edu

³Department of Astronomy, University of Michigan, Ann Arbor, MI 48109, USA

1. Introduction

Carbon is exclusively formed in the hot interiors of stars through the fusion reactions of three alpha particles (i.e., helium nuclei) and expelled into the interstellar space through stellar outflows and/or supernova explosions in the late stages of stellar evolution. As the fourth most abundant element in the universe (by mass) after hydrogen, helium, and oxygen, carbon plays an important role in the physical and chemical evolution of the interstellar medium (ISM; Henning & Salama 1998). Due to its unique property to form three different types of chemical bonds through sp^1 , sp^2 , and sp^3 hybridizations, carbon can be stabilized in various multi-atomic structures with different molecular configurations called allotropes, including amorphous carbon, graphite, diamond, polycyclic aromatic hydrocarbon (PAH), fullerenes, graphene, and carbon nanotubes.

Many allotropes of carbon are known to be present in the ISM (e.g., see Jäger et al. 2011). Presolar graphite grains and nanodiamonds have been identified in primitive meteorites based on their isotopically anomalous composition. These presolar grains were originally condensed in the cooling outflows from carbon-rich evolved stars or in the ejecta of supernovae. They were then expelled into the ISM and eventually made their way into the parental molecular cloud of the Sun and incorporated into asteroids, the parent bodies of meteorites. Therefore, prior to their incorporation into asteroids during the early stages of solar system formation, presolar grains must have had a sojourn in the ISM (see Li & Mann 2012). While hydrogenated amorphous carbon (HAC) grains reveal their presence in the diffuse ISM through the ubiquitous $3.4\mu\text{m}$ aliphatic C–H absorption feature (Pendleton & Allamandola 2002), the aromatic C–H and C–C emission features at 3.3, 6.2, 7.7, 8.6 and $11.3\mu\text{m}$ infer the widespread presence of PAHs in a wide variety of interstellar regions (e.g., see Tielens 2008). The detections of interstellar C_{60} and C_{70} and their cations have also been reported based on their characteristic infrared (IR) emission features, e.g., the 7.0, 8.45, 17.3 and $18.9\mu\text{m}$ features of C_{60} (Cami et al. 2010, Sellgren et al. 2010, Zhang & Kwok 2011, Berné et al. 2017, García-Hernández et al. 2010) and the 6.4, 7.1, 8.2 and $10.5\mu\text{m}$ features of C_{60}^+ (Berné et al. 2013, Strelnikov et al. 2015). In addition, C_{60}^+ has also been suggested as a promising carrier of the mysterious diffuse interstellar bands at 9348.4, 9365.2, 9427.8, 9577.0, and 9632.1 Å (Foing & Ehrenfreund 1994, Campbell et al. 2015, 2016, Walker et al. 2015).

Graphene was first synthesized in the laboratory in 2004 by A.K. Geim and K.S. Novoselov (see Novoselov et al. 2004) for which they received the 2010 Nobel Prize in physics.¹ More

¹We should note that, prior to the work of A.K. Geim and K.S. Novoselov, the Jena Laboratory Astrophysics Group had already successfully synthesized graphene (e.g., see Henning et al. 2004).

recently, García-Hernández et al. (2011b, 2012) reported for the first time the presence of unusual IR emission features at ~ 6.6 , 9.8 , and $20\ \mu\text{m}$ in several planetary nebulae (PNe), both in the Milky Way and the Magellanic Clouds, which are coincident with the strongest transitions of planar C_{24} , a piece of graphene. If confirmed, this would be the first detection of graphene in space. In principle, graphene could be present in the ISM as it could be formed from the photochemical processing of PAHs, which are abundant in the ISM, through a complete loss of their H atoms (e.g., see Berné & Tielens 2012). Chuvilin et al. (2010) showed experimentally that C_{60} could be formed from a graphene sheet. Berné & Tielens (2012) further proposed that such a formation route could occur in space. On the other hand, if there exists in the ISM a population of HAC-like nanoparticles with a mixed aromatic/aliphatic structure (e.g., see Kwok & Zhang 2011), a complete loss of their H atoms could also convert HAC-like nanoparticles into graphene (e.g., see García-Hernández et al. 2010, 2011a,b). Also, graphene could be generated in the ISM from the exfoliation of graphite as a result of grain-grain collisional fragmentation. It is worth noting that graphite is thought to be a major dust component in the ISM (Draine & Lee 1984) and as mentioned earlier, presolar graphite grains have been identified in primitive meteorites.

Both quantum-chemical computations and laboratory experiments have shown that the exciton-dominated electronic transitions in graphene cause a strong absorption band near $2755\ \text{\AA}$ (Yang et al. 2009, Nelson et al. 2010, Trevisanutto et al. 2010) which is not seen in the ISM. In this work, we aim at placing a quantitative upper limit on the abundance of interstellar graphene on the basis of the nondetection of the fingerprint $2755\ \text{\AA}$ absorption feature in the diffuse ISM. To achieve this, we first calculate in §2 the UV absorption of graphene and compare it with the Galactic interstellar extinction curve. Also, if graphene is present in the diffuse ISM, single-photon heating by starlight (Draine & Li 2001) will cause it to radiate in the IR through its characteristic vibrational transitions (e.g., see García-Hernández et al. 2011b, Mackie et al. 2015). Therefore, we calculate in §3 the IR emission spectrum of graphene heated by starlight, and compare it with measurements of the IR emission of the diffuse ISM by the *Infrared Telescope in Space* (IRTS; Onaka et al. 1996) and by the *Diffuse Infrared Background Experiment* (DIRBE; Arendt et al. 1998) and the *Far Infrared Absolute Spectrophotometer* (FIRAS; Finkbeiner et al. 1999) instruments on the *Cosmic Background Explorer* (COBE) satellite. The major conclusion is summarized in §4.

2. UV Absorption

For a planar graphene, the absorption cross section $C_{\text{abs}}(\lambda)$ at wavelength λ per unit volume (V) can be derived from the dielectric function ε as follows (see Yang et al. 2009):

$$C_{\text{abs}}(\lambda)/V = (2\pi/\lambda) \text{Im} \{\varepsilon - 1\} \quad , \quad (1)$$

where $\text{Im} \{\dots\}$ denotes the imaginary part of a complex function. Nelson et al. (2010) employed spectroscopic ellipsometry to measure the complex refractive indices, $m(\lambda) = m' + i m''$ of graphene in the wavelength range of $0.153 < \lambda < 0.783 \mu\text{m}$ or $1.28 < \lambda^{-1} < 6.54 \mu\text{m}^{-1}$. We first convert the refractive indices of graphene measured by Nelson et al. (2010) to complex dielectric functions $\varepsilon = \varepsilon' + i \varepsilon'' = m^2$ (see Figure 1). The Galactic interstellar extinction curve has been relatively well determined from the near-IR at $\lambda^{-1} \lesssim 1 \mu\text{m}^{-1}$ to the far-UV at $\lambda^{-1} \approx 10 \mu\text{m}^{-1}$, over a wavelength range *wider* than that of Nelson et al. (2010). To facilitate a direct comparison of the absorption of graphene with the interstellar extinction curve, an extrapolation of the dielectric functions of Nelson et al. (2010) over a wide wavelength range is needed. To this end, we fit the dielectric functions of Nelson et al. (2010) with three Lorentz oscillators (see Bohren & Huffman 1983):

$$\varepsilon'(\omega) = \varepsilon_0 + \sum_{j=1}^3 \frac{\omega_{p,j}^2 (\omega_{0,j}^2 - \omega^2)}{(\omega_{0,j}^2 - \omega^2)^2 + \gamma_j^2 \omega^2} \quad , \quad (2)$$

$$\varepsilon''(\omega) = \sum_{j=1}^3 \frac{\omega_{p,j}^2 \gamma_j \omega}{(\omega_{0,j}^2 - \omega^2)^2 + \gamma_j^2 \omega^2} \quad , \quad (3)$$

where $\omega = 2\pi c/\lambda$ is the angular frequency, c is the speed of light, $\omega_{p,j}$, $\omega_{0,j}$, and γ_j are respectively the plasma frequency, resonant frequency, and damping constant of the j -th oscillator, and ε_0 is the dielectric function at high frequencies (i.e., $\omega \gg \omega_0$). As illustrated in Figure 1, with $\varepsilon_0 \approx 1.71$ and three Lorentz oscillators characterized by $\omega_{p,1} \approx 7.79 \times 10^{15}$ GHz, $\omega_{0,1} \approx 6.89 \times 10^{15}$ GHz, $\gamma_1 \approx 1.52 \times 10^{15}$ GHz, $\omega_{p,2} \approx 16.47 \times 10^{15}$ GHz, $\omega_{0,2} \approx 1.61 \times 10^{15}$ GHz, $\gamma_2 \approx 13.99 \times 10^{15}$ GHz, $\omega_{p,3} \approx 10.58 \times 10^{15}$ GHz, $\omega_{0,3} \approx 6.33 \times 10^{15}$ GHz, $\gamma_3 \approx 5.18 \times 10^{15}$ GHz, we are able to closely fit the dielectric functions of graphene experimentally derived by Nelson et al. (2010). Eqs. 2 and 3 allow us to extrapolate the dielectric functions of graphene at $\lambda^{-1} < 1.28 \mu\text{m}^{-1}$ and $\lambda^{-1} > 6.54 \mu\text{m}^{-1}$.²

²This extrapolation is physical since it is based on a simple physical principle (i.e., the classical Lorentz harmonic oscillator model). Even if this extrapolation is not accurate, it does not affect the following discussion on its contribution to the interstellar extinction since the absorption of graphene occurs mostly at $2 < \lambda^{-1} < 6 \mu\text{m}^{-1}$. Also because of this, it will not affect the following discussion on its IR emission.

For graphene, we can relate its volume (V) to the number of C atoms (N_C), through

$$\frac{V}{N_C} = \frac{12 m_H d}{\sigma} , \quad (4)$$

where $m_H \approx 1.66 \times 10^{-24}$ g is the mass of a hydrogen nuclei, $d \approx 3.4 \text{ \AA}$ is the monolayer thickness of graphene, and $\sigma \approx 6.5 \times 10^{-8} \text{ g cm}^{-2}$ is the surface mass density of graphene. Combining eq. 1 with eq. 4, we obtain the absorption cross section of graphene per C atom from

$$C_{\text{abs}}(\lambda)/N_C = \frac{24\pi m_H d}{\sigma \lambda} \text{Im} \{\varepsilon - 1\} . \quad (5)$$

In Figure 2 we show the UV/optical absorption cross section (per C atom) of graphene. Most prominent in the absorption profile of graphene is the exciton-dominated absorption peak at $\sim 4.5 \text{ eV}$ (i.e, $\lambda \approx 2755 \text{ \AA}$, $\lambda^{-1} \approx 3.63 \mu\text{m}^{-1}$). We note that quantum-chemical first-principles calculations of many-electron effects on the optical response of graphene have also demonstrated that the resonant excitons give rise to a prominent peak in the absorption spectrum of graphene near 4.5 eV (see Yang et al. 2009, Trevisanutto et al. 2010). However, this absorption peak is absent in the interstellar extinction curve. As shown in Figure 3, the Galactic extinction curve — the variation of the extinction A_λ with the inverse wavelength λ^{-1} — rises almost linearly from the near-IR to the near-UV, with a broad absorption bump at about $\lambda^{-1} \approx 4.6 \mu\text{m}^{-1}$ ($\lambda \approx 2175 \text{ \AA}$) and followed by a steep rise into the far-UV at $\lambda^{-1} \approx 10 \mu\text{m}^{-1}$, the shortest wavelength at which the dust extinction has been measured (Mathis 1990, Fitzpatrick 1999). The nondetection of the 2755 \AA absorption feature allows us to place an upper limit on the abundance of graphene in the ISM.

Weingartner & Draine (2001) and Li & Draine (2001b) have developed a carbonaceous-silicate grain model which reproduces both the observed Galactic extinction curve and the observed IR emission. In Figure 3 we show the extinction obtained by *adding* graphene to this model. Since graphene is in the Rayleigh limit, the added extinction depends only on $[\text{C}/\text{H}]_{\text{graph}}$, the amount of C (relative to H) tied up in graphene, and is independent of the exact graphene size:

$$\left(\frac{A_\lambda}{N_H} \right)_{\text{graph}} = 1.086 \left(\frac{C_{\text{abs}}}{N_C} \right)_{\text{graph}} [\text{C}/\text{H}]_{\text{graph}} . \quad (6)$$

As shown in Figure 3, the red wing of the strong 2175 \AA extinction bump could hide certain amount of graphene: we estimate the upper bound to be $[\text{C}/\text{H}]_{\text{graph}} \approx 5 \text{ ppm}$ — i.e., in

After all, graphene absorbs little at $\lambda^{-1} < 1.28 \mu\text{m}^{-1}$ and $\lambda^{-1} > 6.54 \mu\text{m}^{-1}$ and therefore the existing, experimentally-derived dielectric function data at $1.28 < \lambda^{-1} < 6.54 \mu\text{m}^{-1}$ are sufficient for determining the heating of graphene.

the diffuse ISM there could be as much as ~ 5 ppm of C/H in graphene for the characteristic 2755 \AA absorption feature of graphene to remain unnoticeable. The contribution of graphene to the $\lambda^{-1} \sim 3.6 \mu\text{m}^{-1}$ region would be considerable for $[\text{C}/\text{H}]_{\text{graph}} > 6$ ppm. If we take the interstellar C abundance to be solar-like (i.e., $\text{C}/\text{H} \approx 269 \pm 31$ ppm, Asplund et al. 2009), an upper limit of $[\text{C}/\text{H}]_{\text{graph}} \approx 5$ ppm implies that at as much as $\sim 1.9\%$ of the interstellar C atoms could be tied up in graphene.

3. IR Emission

For a planar graphene of several hundred C atoms or smaller, photon absorption is often the dominant excitation process and its energy content is often smaller than the energy of a single starlight photon. Therefore, graphene will undergo stochastic heating in the ISM (Greenberg 1968). In most cases soon after the photoabsorption, graphene will convert almost all of the initial photoexcitation energy to vibrational energy of the highly vibrationally excited ground electronic state, and hence IR emission is always the dominant relaxation process (e.g., see Li 2004). Therefore, we will model the stochastic heating of graphene in terms of pure vibrational transitions by employing the “exact-statistical” method of Draine & Li (2001).

Following Draine & Li (2001), we characterize the state of a graphene sheet of N_{C} C atoms by its vibrational energy E , and group its energy levels into $(M+1)$ “bins”, where the j -th bin ($j=0, \dots, M$) is $[E_{j,\text{min}}, E_{j,\text{max}})$, with representative energy $E_j \equiv (E_{j,\text{min}} + E_{j,\text{max}})/2$, and width $\Delta E_j \equiv (E_{j,\text{max}} - E_{j,\text{min}})$. Let P_j be the probability of finding the graphene sheet of N_{C} C atoms in bin j with energy E_j . The probability vector P_j evolves according to

$$dP_i/dt = \sum_{j \neq i} \mathbf{T}_{ij} P_j - \sum_{j \neq i} \mathbf{T}_{ji} P_i \quad , \quad i = 0, \dots, M \quad , \quad (7)$$

where the transition matrix element \mathbf{T}_{ij} is the probability per unit time for graphene in bin j to make a transition to one of the levels in bin i . We solve the steady state equations

$$\sum_{j \neq i} \mathbf{T}_{ij} P_j = \sum_{j \neq i} \mathbf{T}_{ji} P_i \quad , \quad i = 0, \dots, M \quad (8)$$

to obtain the $M+1$ elements of P_j , and then calculate the resulting IR emission spectrum (see eq. 55 of Draine & Li 2001).

Before we proceed to calculate the state-to-state transition rates \mathbf{T}_{ji} for transitions $i \rightarrow j$, let's distinguish the excitation rates \mathbf{T}_{ul} (from l to u , $l < u$) from the deexcitation rates \mathbf{T}_{lu} (from u to l , $l < u$). For a given starlight energy density u_E , the rates for upward transitions

$l \rightarrow u$ (i.e., the excitation rates) are just the photon absorption rates:

$$\mathbf{T}_{ul} \approx C_{\text{abs}}(E) c u_E \Delta E_u / (E_u - E_l) \quad . \quad (9)$$

The rates for downward transitions $u \rightarrow l$ (i.e., the deexcitation rates) can be determined from the detailed balance analysis of the Einstein A coefficient:

$$\mathbf{T}_{lu} \approx \frac{8\pi}{h^3 c^2} \frac{g_l}{g_u} \frac{\Delta E_u}{E_u - E_l} E^3 \times C_{\text{abs}}(E) \left[1 + \frac{h^3 c^3}{8\pi E^3} u_E \right] \quad , \quad (10)$$

where h is the Planck constant, and the degeneracies g_u and g_l are the numbers of energy states in bins u and l , respectively:

$$g_j \equiv N(E_{j,\text{max}}) - N(E_{j,\text{min}}) \approx (dN/dE)_{E_j} \Delta E_j \quad , \quad (11)$$

where $(dN/dE)_{E_j}$ is the vibrational density of states of graphene at internal energy E_j . For a planar graphene sheet of N_C C atoms, if we know the frequencies of all its $(3N_C - 6)$ vibrational modes, we can employ the Beyer-Swinehart numerical algorithm (Beyer & Swinehart 1973, Stein & Rabinovitch 1973) to calculate the vibrational density of states $(dN/dE)_{E_j}$ and therefore the degeneracies g_j for each vibrational energy bin. If we know the oscillator strength of each vibrational mode, we can obtain the IR absorption cross section $C_{\text{abs}}(E)$ of graphene by summing up all the vibrational transitions with each approximated as a Drude profile.

Mackie et al. (2015) computed the vibrational transitions of 805 fully dehydrogenated PAHs, using the B3LYP density functional theory (DFT), together with the 4-31G basis set (Frisch et al. 1984). These molecules span a wide range of sizes, from two benzene rings up to eight rings, with the largest one containing 34 C atoms. Although the individual spectra of these fully dehydrogenated species are rather diverse, as a whole they do show characteristic features at 5.2, 5.5, and 10.6 μm as well as a forest of features in the $\sim 16\text{--}30 \mu\text{m}$ range that appears as a structured continuum, but with a clear peak centered around 19 μm . However, we note that not all of these fully dehydrogenated PAHs are planar or graphene-like. Also, a complete set of the frequencies of all the $(3N_C - 6)$ vibrational modes computed by Mackie et al. (2015) for each individual species of N_C C atoms is not yet publicly available. This prevents us from computing the IR emission spectra of the graphene-like species considered by Mackie et al. (2015). This is because, to calculate the vibrational density of states (see eq. 11), for a given species of N_C C atoms a complete knowledge of the frequencies of all the $(3N_C - 6)$ vibrational modes is required. On the other hand, in the literature the vibrational modes and intensities are known for C_{24} , a small graphene sheet. Martin et al. (1996) performed quantum-chemical computations for C_{24} using the B3LYP DFT. Kuzmin & Duley (2011) also carried out DFT-based calculations for planar C_{24} and obtained similar

results. In this work, we will therefore consider the vibrational excitation and the subsequent IR emission of C_{24} . We note that C_{24} is preferred also because it has been possibly detected in several Galactic and extragalactic PNe (García-Hernández et al. 2011a, 2012) and even in the ISM (Berné et al. 2013).³

We consider the stochastic heating of C_{24} in the diffuse ISM, excited by the solar neighbourhood interstellar radiation field (ISRF) estimated by Mathis et al. (1983; hereafter MMP83). We consider 500 energy bins (i.e., $M = 500$). We use the vibrational modes and intensities of C_{24} computed by Martin et al. (1996) to calculate the vibrational density of states and the degeneracies for each vibrational energy bin as well as the IR absorption cross section. Without a prior knowledge of the width of each vibrational transition, we assign a width of 30 cm^{-1} , consistent with the natural line width expected from free-flying molecule (see Allamandola et al. 1989). This natural line width arises from intramolecular vibrational energy redistribution. In Figure 2 we show the IR absorption cross section of graphene based on the quantum-chemical data of C_{24} which clearly exhibits three strong IR bands at 6.6, 9.8 and $20 \mu\text{m}$.

With g_j and $C_{\text{abs}}(E)$ derived from C_{24} of Martin et al. (1996) and the starlight energy density u_E taken from MMP83, we determine the state-to-state transition rates \mathbf{T}_{ji} and solve the steady-state probability evolution equation to obtain the steady-state energy probability distribution P_j and finally calculate the resulting IR emission spectrum. In Figure 4 we show the IR emission of C_{24} excited by the MMP83 ISRF. Most pronounced are the IR emission features at 6.6, 9.8 and $20 \mu\text{m}$. We note that the sawtooth features at $\lambda > 30 \mu\text{m}$ are artificial; they are due to our treatment of transitions from the lower excited energy bins to the ground state and first few excited states (see Draine & Li 2001).

We will now derive upper limits on the abundance of graphene in the diffuse ISM based on comparison of the observed IR emission with the calculated emission spectrum of C_{24} . We first consider the high Galactic-latitude (HGL) cirrus illuminated by the MMP83 ISRF. The average emission per H for the HGL region has been measured by *COBE*/DIRBE (Arendt et al. 1998), *COBE*/FIRAS (Finkbeiner et al. 1999), and *Planck* (Planck Collaboration XVII 2014). As shown in Figure 5a, with 5 ppm of C/H in graphene C_{24} , the 6.6, 9.8 and $20 \mu\text{m}$ emission features of graphene will become so prominent that they will be essentially as strong as the PAH features at 6.2, 7.7, 8.6 and $11.3 \mu\text{m}$ and would have been detected by *Spitzer* or by the *Short Wavelength Spectrometer* (SWS) aboard the *Infrared Space Observatory* (ISO).

Following Li & Draine (2001a), we have also considered the diffuse ISM toward $l =$

³Berné et al. (2013) reported the detection in NGC 7023, a reflection nebula, of the $6.6 \mu\text{m}$ band coincident with the assignment of C_{24} made by García-Hernández et al. (2011a).

$44^{\circ}20'$, $b = -0^{\circ}20'$ which has been observed by *COBE/DIRBE* (Hauser et al. 1998) and the *Mid-Infrared Spectrograph* (MIRS) aboard *IRTS* has obtained the $4.7\text{--}11.7\mu\text{m}$ spectrum (Onaka et al. 1996). Li & Draine (2001b) have modeled the IR emission from the dust in this direction and derived a total gas column $N_{\text{H}} \approx 4.3 \times 10^{22} \text{ cm}^{-2}$ and a starlight intensity of $U \approx 2$ (in unit of the MMP83 ISRF). As illustrated in Figure 5b, if graphene C_{24} is present in this region, its abundance must be less than 5 ppm of C/H, otherwise the 6.6, 9.8 and $20\mu\text{m}$ emission features of graphene would have been detected by *IRTS*. Therefore, for both the HGL region and the line of sight toward $l = 44^{\circ}20'$, $b = -0^{\circ}20'$, a generous upper limit of $\text{C}/\text{H} \lesssim 5 \text{ ppm}$ is imposed by the *COBE/DIRBE* photometric data and the *IRTS* spectrum.

4. Summary

Inspired by the possible detection of the 6.6, 9.8 and $20\mu\text{m}$ emission features of graphene C_{24} in several Galactic and extragalactic PNe, we have explored how much graphene could be present in the diffuse ISM and how it would reveal its presence through absorption and emission. We have placed an upper limit of $\sim 5 \text{ ppm}$ of C/H on the abundance of graphene in the diffuse ISM, based on the nondetection in the Galactic interstellar extinction curve of the prominent absorption peak at $\sim 2755 \text{ \AA}$ of graphene caused by resonant excitons as well as the nondetection of the 6.6, 9.8, and $20\mu\text{m}$ emission features of graphene C_{24} in the observed IR emission spectra of the diffuse ISM. While the extinction-based constraint is size-independent as long as graphene is in the Rayleigh regime, the IR-emission-based constraint is sensitive to the graphene size since the stochastic heating and the resulting IR emission spectrum depend on the graphene size. Further quantum-chemical computations and experimental measurements of the IR vibrational spectra of graphene of a wide range of sizes as well as the vibrational excitation modeling of the IR emission of graphene in various astrophysical regions will be crucial to more rigorously explore the presence and quantity of graphene in space.

We thank B.T. Draine, W.W. Duley, D.A. García-Hernández, Th. Hening, C. Jäger, S. Kuzmin, F.Y. Xiang, L. Yang, X.J. Yang, J.X. Zhong, and the anonymous referee for very helpful discussions and suggestions. This work is supported by NSFC through Projects 11173007, 11373015, 11533002, and 973 Program 2014CB845702. AL is supported in part by NSF AST-1311804 and NASA NNX14AF68G.

REFERENCES

- Allamandola, L.J., Tielens, A.G.G.M., & Barker, J.R. 1989, *ApJS*, 71, 733
- Arendt, R. G., Odegard, N., Weiland, J. L., et al. 1998, *ApJ*, 508, 74
- Asplund, M., Grevesse, N., Sauval, A. J., & Scott, P. 2009, *ARA&A*, 47, 481
- Berné, O., & Tielens, A.G.G.M. 2012, *PNAS*, 109, 401
- Berné, O., Mulas, G., & Joblin, C. 2013, *A&A*, 550, L4
- Berné, O., Cox, N. L. J., Mulas, G., & Joblin, C. 2017, *A&A*, 605, L1
- Bernstein, L. S., Shroll, R. M., Lynch, D. K., & Clark, F. O. 2017, *ApJ*, 836, 229
- Beyer, T., & Swinehart, D.F. 1973, *Commun. Assoc. Comput. Machinery*, 16, 379
- Bohren, C.F., & Huffman, D.R. 1983, *Absorption and Scattering of Light by Small Particles*, Wiley, New York
- Campbell, E.K., Holz, M., Gerlich, D., & Maier, J.P. 2015, *Nature*, 523, 322
- Campbell, E.K., Holz, M., & Maier, J.P. 2016, *ApJL*, 826, L4
- Cami, J., Bernard-Salas, J., Peeters, E., & Malek, S. E. 2010, *Science*, 329, 1180
- Chuvilin, A., Kaiser, U., Bichoutskaia, E., Besley, N. A., & Khlobystov, A. N. 2010, *Nature Chem.*, 2, 450
- Draine, B.T., & Lee, H.M. 1984, *ApJ*, 285, 89
- Draine, B.T., & Li, A. 2001, *ApJ*, 551, 807
- Finkbeiner, D. P., Davis, M., & Schlegel, D.J. 1999, *ApJ*, 524, 867
- Fitzpatrick, E.L. 1999, *PASP*, 111, 63
- García-Hernández, D. A., Manchado, A., García-Lario, P., et al. 2010, *ApJL*, 724, L39
- García-Hernández, D. A., Kameswara Rao, N., & Lambert, D. L. 2011a, *ApJ*, 729, 126
- García-Hernández, D. A., Iglesias-Groth, S., Acosta-Pulido, J. A., et al. 2011b, *ApJL*, 737, L30
- García-Hernández, D. A., Villaver, E., García-Lario, P., et al. 2012, *ApJ*, 760, 107

- Greenberg, J.M. 1968, in *Stars and Stellar Systems*, Vol. VII, ed. B.M. Middlehurst & L.H. Aller (Chicago: Univ. of Chicago Press), 221
- Hauser, M.G., Kelsall, T., Leisawitz, D., & Weiland, J. 1998, COBE Diffuse Infrared Background Experiment Explanatory Supplement version 2.3 (COBE Ref. Pub. No. 98-A; Greenbelt: NASA/GSFC)
- Henning, Th., & Salama, F. 1998, *Science*, 282, 2204
- Henning, Th., Jäger, C., & Mutschke, H. 2004, in *Astrophysics of Dust* (ASP Conf. Ser. 309), ed. A.N. Witt, G.C. Clayton, & B.T. Draine (San Francisco, CA: ASP), 603
- Jäger, C., Mutschke, H., Henning, Th., & Huisken, F. 2011, *EAS Publ. Ser.*, 46, 293
- Kuzmin, S., & Duley, W. W. 2011, arXiv:1103.2989
- Kwok, S., & Zhang, Y. 2011, *Nature*, 479, 80
- Li, A. 2004, *Astrophysics of Dust* (ASP Conf. Ser. 309), ed. A.N. Witt, G.C. Clayton, & B.T. Draine (San Francisco, CA: ASP), 417
- Li, A., & Draine, B.T. 2001a, *ApJL*, 550, L213
- Li, A., & Draine, B.T. 2001b, *ApJ*, 554, 778
- Li, A., & Mann, I. 2012, in *Astrophys. Space Sci. Library*, Vol. 385, *Nanodust in the Solar System: Discoveries and Interpretations* (Berlin: Springer-Verlag), 5
- Mackie, C. J., Peeters, E., Bauschlicher, C. W., Jr., & Cami, J. 2015, *ApJ*, 799, 131
- Martin, J. M. L., El-Yazal, J., & François, J.-P. 1996, *Chem. Phys. Lett.*, 255, 7
- Mathis, J.S. 1990, *ARA&A*, 28, 37
- Mathis, J.S., Mezger, P.G., & Panagia, N. 1983, *A&A*, 128, 212
- Nelson, F. J., Kamineni, V. K., Zhang, T., et al. 2010, *Appl. Phys. Lett.*, 97, 253110
- Novoselov, K. S., Geim, A. K., Morozov, S. V., et al. 2004, *Science*, 306, 666
- Onaka, T., Yamamura, I., Tanabe, T., et al. 1996, *PASJ*, 48, L59
- Pendleton, Y. J., & Allamandola, L. J. 2002, *ApJS*, 138, 75
- Planck Collaboration XVII 2014, *A&A*, 566, A55

- Sellgren, K., Werner, M. W., Ingalls, J. G., et al. 2010, *ApJL*, 722, L54
- Stecher, T.P., & Donn, B. 1965, *ApJ*, 142, 1681
- Stein, S.E., & Rabinovitch, B.S. 1973, *J. Chem. Phys.*, 58, 2438
- Strelnikov, D., Kern, B., & Kappes, M. M. 2015, *A&A*, 584, A55
- Tielens, A. G. G. M. 2008, *ARA&A*, 46, 289
- Trevisanutto, P.E., Holzmann, M., Côté, M., & Olevano, V. 2010, *Phys. Rev. B*, 81, 121405
- Walker, G.A.H., Bohlender, D. A., Maier, J. P., & Campbell, E. K. 2015, *ApJL*, 812, L8
- Weingartner, J.C., & Draine, B.T. 2001, *ApJ*, 548, 296
- Yang, L., Deslippe, J., Park, C.-H., Cohen, M. L., & Louie, S. G. 2009, *Phys. Rev. Lett.*, 103, 186802
- Zhang, Y., & Kwok, S. 2011, *ApJ*, 730, 126

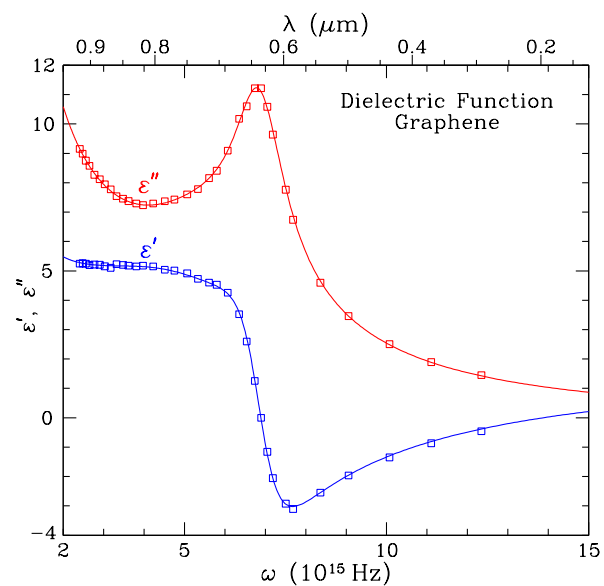


Fig. 1.— Real (ϵ') and imaginary (ϵ'') parts of the dielectric function of graphene. Open squares: experimental data of Nelson et al. (2010). Solid lines: model fits with three Lorentz oscillators.

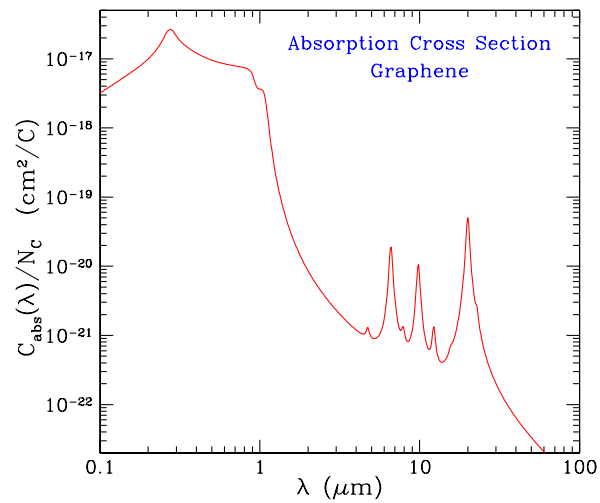


Fig. 2.— Absorption cross sections (per C atom) of graphene from the far-UV to the IR. Following Li & Draine (2001b), we smoothly join the UV part and the IR part.

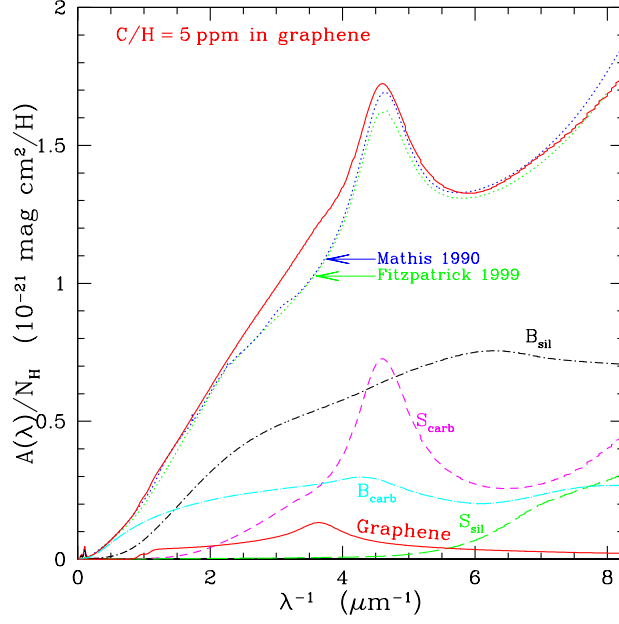


Fig. 3.— Comparison of the average Galactic interstellar extinction curve (open circles: Mathis 1990; dotted line: Fitzpatrick 1999) with the model extinction curve (solid red line) obtained by adding the contribution from graphene with $[C/H]_{\text{graph}} = 5$ ppm (thin red line) to the best-fit model of Weingartner & Draine (2001). Also plotted are the contributions (see Li & Draine 2001b) from “ B_{sil} ” ($a \geq 250\text{\AA}$ silicate); “ S_{sil} ” ($a < 250\text{\AA}$ silicate); “ B_{carb} ” ($a \geq 250\text{\AA}$ carbonaceous); “ S_{carb} ” ($a < 250\text{\AA}$ carbonaceous, including PAHs).

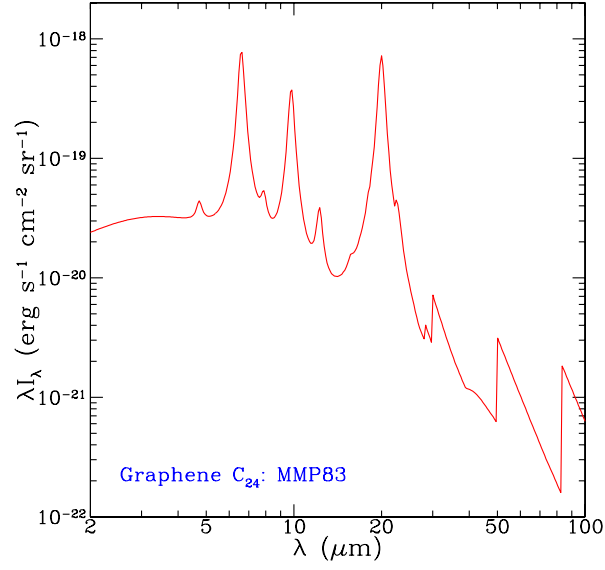


Fig. 4.— IR emission spectrum of graphene of $N_C = 24$ illuminated by the MMP83 ISRF. The sawtooth features at $\lambda > 30 \mu\text{m}$ are due to our treatment of transitions from the lower excited energy bins to the ground state and first few excited states (see Draine & Li 2001).

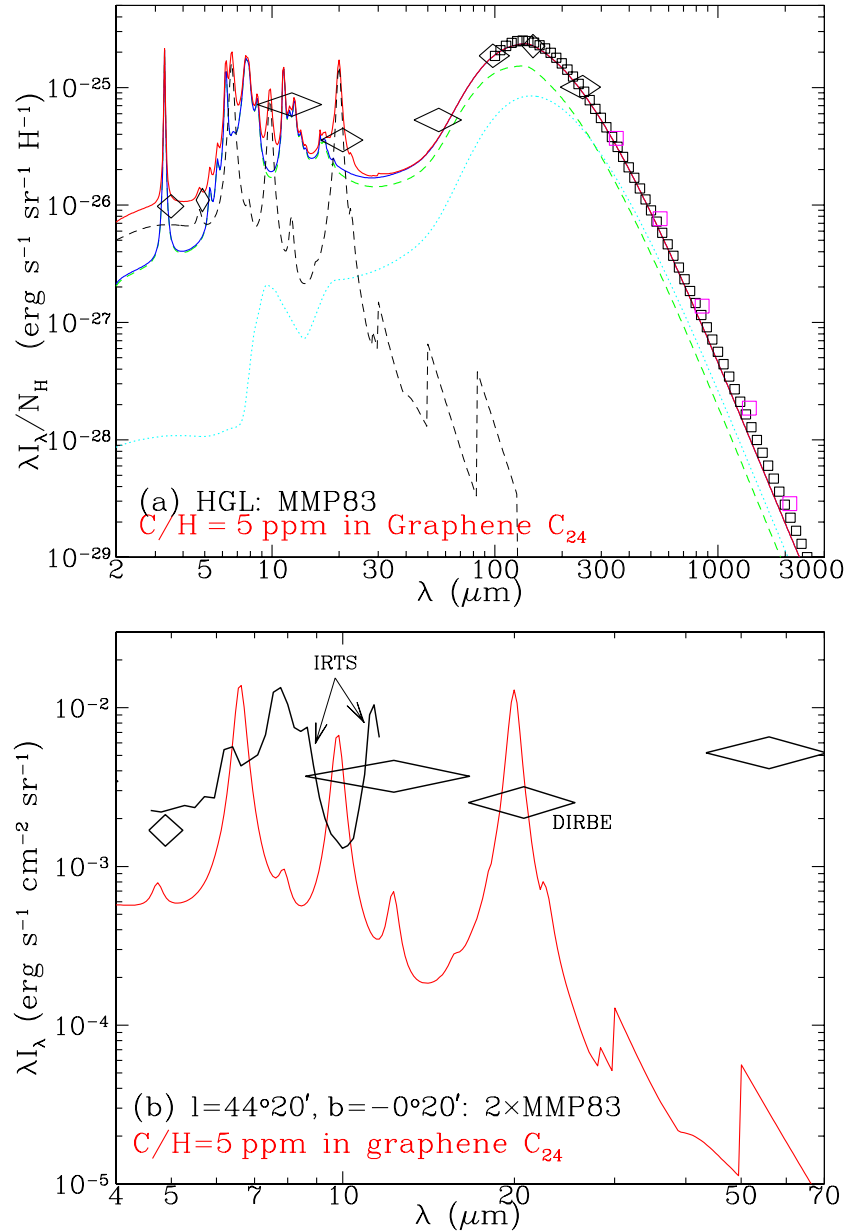


Fig. 5.— Upper panel (a): Comparison of the observed IR emission from the HGL cirrus with the model emission spectrum obtained by adding the contribution from graphene C₂₄ of [C/H]_{graph} = 5 ppm (black dashed line) to the best-fit model of Li & Draine (2001b) which consists of contributions from amorphous silicate (cyan dotted line) and carbonaceous grains (i.e., graphite and PAHs; green dashed line). The sum of amorphous silicate and carbonaceous grains is shown as blue solid line. Observational data are from *DIRBE* (black diamonds; Arendt et al. 1998), *FIRAS* (black squares; Finkbeiner et al. 1999), and *Planck* (magenta squares; Planck Collaboration XVII 2014). Bottom panel (b): Contribution to the IR emission toward (44° ≤ *l* ≤ 44°40', -0°40' ≤ *b* ≤ 0°) by graphene C₂₄ of [C/H]_{graph} = 5 ppm (solid red line). Diamonds: *DIRBE* photometry. Black solid line: 5–12 μm spectrum observed by IRTS (Onaka et al. 1996).